Modelling Simul. Mater. Sci. Eng. 2 (1994) 739–754. Printed in the UK

Mechanical modelling of grain boundary sliding of polycrystals

T C Wang and W K Pan

LNM, Institute of Mechanics, Chinese Academy of Sciences, Beijing 100 080, People's Republic of China

Received 4 November 1993, accepted for publication 4 November 1993

Abstract. Using a variational method, a general three-dimensional solution to the problem of a sliding spherical inclusion embedded in an infinite anisotropic medium is presented in this paper. The inclusion itself is also a general anisotropic elastic medium. The interface is treated as a thin interface layer with interphase anisotropic properties. The displacements in the matrix and the inclusion are expressed as polynomial series of the cartesian coordinate components. Using the virtual work principle, a set of linear algebraic equations about unknown coefficients are obtained. Then the general sliding spherical inclusion problem is accurately solved. Based on this solution, a self-consistent method for sliding polycrystals is proposed. Combining this with a two-dimensional model of an aggregate polycrystal, a systematic analysis of the mechanical behaviour of sliding polycrystals is given in detail. Numerical results are given to show the significant effect of grain boundary sliding on the overall mechanical properties of aggregate polycrystals.

1. Introduction

Theoretical prediction of the elastic–plastic behaviour of polycrystalline materials on the basis of single-crystal properties has played an important role in the field of physical theories of plasticity [1–5]. The finite element method provides a direct numerical solution of a boundary value problem which takes account of interaction between grains.

A semi-analytical method is used out on the basis of some averaging techniques. A powerful averaging scheme is the self-consistent method, originally proposed by Kröner [6], and Budiansky and Wu [7] and elaborated by Hill *et al* [1]. However, most of these theories are based on the assumption that the interfacial displacements and tractions across the boundary must be continuous.

The assumption of perfect bonding is sometimes inadequate. The interface damage due to cyclic loading, thermo-impact, high-temperature, intensive deformation and chemical interaction is a common phenomenon. Grain boundary sliding in granular media like rock, soil, sand, etc, is also a common feature.

Recently, the new technology of thin coating on reinforcement particles and fibres has been widely used. This has resulted in considerable interest in imperfect interface conditions.

Inclusion problems with imperfect interface have been treated by Walpole [8], Mura *et al* [9], Ghahremani [10], Benvenise [11], Hashin [12], Luo and Weng [13], and Luo and Chen [14] among others. But most works only deal with an inclusion which is embedded in an infinite isotropic elastic medium. Up to now, very few works have considered the effect of interface damage on the overall behaviour of aggregate polycrystals. Yang *et al*

0965-0393/94/3A0739+16$19.50

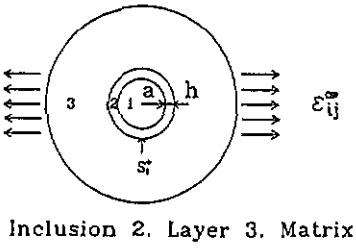

Figure 1. Calculation model. 1. Inclusion. 2. Layer. 3. Matrix.

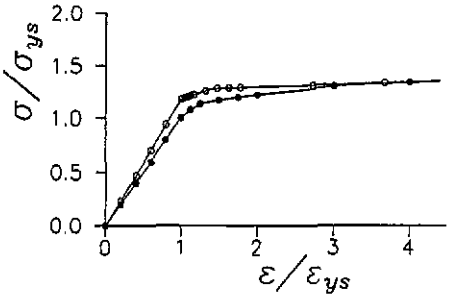

Figure 2. Tensile stress–strain curves of 2D (O) and 3D (●) Hill's model with non-hardening single crystal.

[15] have given a stress–strain relation of a sliding polycrystal, assuming perfect normal interface bonding and ideally tangential free sliding.

A general solution of a sliding spherical inclusion which is embedded in an infinite anisotropic medium is presented in this paper. Using this solution, a self-consistent model for sliding polycrystals is proposed. A systematic analysis of the mechanical behaviour of sliding polycrystals is given in detail.

2. Sliding spherical inclusion

Consider an infinite anisotropic elastic body containing a spherical inclusion in a domain Ω. The infinite body is subject to uniform stresses at infinity. The remote displacement field u_i is

$$u_i = \varepsilon_{ij}^\infty x_j \qquad \text{when } r \to \infty. \tag{1}$$

The spherical inclusion with radius a is also a general anisotropic elastic medium. The interface is treated as an interface layer with inner radius a and outer radius R ($R = a + h$). Suppose the thickness h of the interface layer to be very small ($h \ll a$). The strain components in the interface layer can be approximately expressed as

$$\varepsilon_r \doteq [u_r]/h \qquad \gamma_{r\theta} \doteq [u_\theta]/h \qquad \gamma_{r\phi} \doteq [u_\phi]/h. \tag{2}$$

Other strain components are assumed to be negligibly small in comparison with the above components.

It is a very hard task to derive an analytical solution using the Green's function of an anisotropic elasticity for the present three-phase boundary problem. In order to get an analytical solution, the variational method is employed in this paper.

The virtual work principle, which is equivalent to the equilibrium equation in the body and the traction condition on the surface, is given by

$$\delta\Pi = \delta U_1 + \delta U_2 + \int_{V_3} (\sigma_{ij} - \sigma_{ij}^\infty)\delta\varepsilon_{ij}\,\mathrm{d}V + \int_{S_i^+} \sigma_{ij}^\infty n_i \delta u_j\,\mathrm{d}S = 0 \tag{3}$$

where U_1 is the elastic strain energy of the inclusion, U_2 is the elastic deformation energy of the interface layer, S_i^+ is the internal surface of the matrix, and V_3 is the volume occupied by the infinite matrix, as shown in figure 1.

The displacements u_i in the inclusion can be represented as

$$u_x = \sum_{m,n,k=0}^{\infty} a_{mnk} x^m y^n z^k$$

$$u_y = \sum_{m,n,k=0}^{\infty} b_{mnk} x^m y^n z^k \tag{4}$$

$$u_z = \sum_{m,n,k=0}^{\infty} c_{mnk} x^m y^n z^k.$$

The strain components of the inclusion are given by

$$\varepsilon_x = \sum_{m,n,k=0}^{\infty} a_{mnk} X_{mnk}(m/x)$$

$$\varepsilon_y = \sum_{m,n,k=0}^{\infty} b_{mnk} X_{mnk}(n/y)$$

$$\varepsilon_z = \sum_{m,n,k=0}^{\infty} c_{mnk} X_{mnk}(k/z) \tag{5}$$

$$\gamma_{yz} = \sum_{m,n,k=0}^{\infty} X_{mnk}[b_{mnk}(k/z) + c_{mnk}(n/y)]$$

$$\gamma_{zx} = \sum_{m,n,k=0}^{\infty} X_{mnk}[c_{mnk}(m/x) + a_{mnk}(k/z)]$$

$$\gamma_{xy} = \sum_{m,n,k=0}^{\infty} X_{mnk}[a_{mnk}(n/y) + b_{mnk}(m/x)].$$

Here

$$X_{mnk} = x^m y^n z^k. \tag{6}$$

Introduce the standard stress vector $\sigma = [\sigma_x, \sigma_y, \sigma_z, \tau_{yz}, \tau_{zx}, \tau_{xy}]^T$ and strain vector $\varepsilon = [\varepsilon_x, \varepsilon_y, \varepsilon_z, \gamma_{yz}, \gamma_{zx}, \gamma_{xy}]^T$.

The elastic constitutive relation for the inclusion is

$$\sigma = g\varepsilon \tag{7}$$

where g_{ij} are the elastic moduli of the inclusion.

The displacements u_i in the matrix take the form

$$u_x = \sum_{m,n,k=0}^{\infty} A_{mnk} x^m y^n z^k / r^{2(m+n+k)} + \varepsilon_{1j}^{\infty} x_j$$

$$u_y = \sum_{m,n,k=0}^{\infty} B_{mnk} x^m y^n z^k / r^{2(m+n+k)} + \varepsilon_{2j}^{\infty} x_j \tag{8}$$

$$u_z = \sum_{m,n,k=0}^{\infty} C_{mnk} x^m y^n z^k / r^{2(m+n+k)} + \varepsilon_{3j}^{\infty} x_j.$$

The strain components ε_{ij} in the matrix are

$$\varepsilon_x = \sum_{m,n,k=0}^{\infty} \frac{A_{mnk}}{r^{2(m+n+k)}} X_{mnk}\left(\frac{m}{x} + \alpha_{mnk}\frac{x}{r^2}\right) + \varepsilon_{11}^{\infty}$$

$$\varepsilon_y = \sum_{m,n,k=0}^{\infty} \frac{B_{mnk}}{r^{2(m+n+k)}} X_{mnk}\left(\frac{n}{y} + \alpha_{mnk}\frac{y}{r^2}\right) + \varepsilon_{22}^{\infty}$$

$$\varepsilon_z = \sum_{m,n,k=0}^{\infty} \frac{C_{mnk}}{r^{2(m+n+k)}} X_{mnk}\left(\frac{k}{z} + \alpha_{mnk}\frac{z}{r^2}\right) + \varepsilon_{33}^{\infty} \tag{9}$$

$$\gamma_{yz} = \sum_{m,n,k=0}^{\infty} \frac{X_{mnk}}{r^{2(m+n+k)}}\left(B_{mnk}\frac{k}{z} + C_{mnk}\frac{n}{y} + \alpha_{mnk}(B_{mnk}z + C_{mnk}y)/r^2\right) + 2\varepsilon_{23}^{\infty}$$

$$\gamma_{zx} = \sum_{m,n,k=0}^{\infty} \frac{X_{mnk}}{r^{2(m+n+k)}}\left(C_{mnk}\frac{m}{x} + A_{mnk}\frac{k}{z} + \alpha_{mnk}(C_{mnk}x + A_{mnk}z)/r^2\right) + 2\varepsilon_{31}^{\infty}$$

$$\gamma_{xy} = \sum_{m,n,k=0}^{\infty} \frac{X_{mnk}}{r^{2(m+n+k)}}\left(A_{mnk}\frac{n}{y} + B_{mnk}\frac{m}{x} + \alpha_{mnk}(A_{mnk}y + B_{mnk}x)/r^2\right) + 2\varepsilon_{12}^{\infty}$$

where $\alpha_{mnk} = -2(m + n + k)$.

The elastic constitutive relation is

$$\sigma = G\varepsilon \tag{10}$$

where G_{ij} are the elastic moduli of the matrix.

For the interface layer, the constitutive relation is

$$\sigma_r = E_r\varepsilon_r \qquad \tau_{r\theta} = G_\theta\gamma_{r\theta} \qquad \tau_{r\phi} = G_\phi\gamma_{r\phi}. \tag{11}$$

Introduce the following notations:

$$\boldsymbol{m} = [m_1\ m_2\ m_3] = [m\ n\ k] \qquad \boldsymbol{p} = [p_1\ p_2\ p_3] = [p\ q\ s]$$

$$X_{\boldsymbol{m}} = X_{mnk} \qquad X_{\boldsymbol{p}} = X_{pqs} \qquad a_{\boldsymbol{m}} = a_{mnk} \qquad A_{\boldsymbol{p}} = A_{pqs}$$

$$\begin{pmatrix} i_1 & i_2 & i_3 \\ j_1 & j_2 & j_3 \end{pmatrix}_g = \begin{bmatrix} g_{i_1j_1} & g_{i_1j_2} & g_{i_1j_3} \\ g_{i_2j_1} & g_{i_2j_2} & g_{i_2j_3} \\ g_{i_3j_1} & g_{i_3j_2} & g_{i_3j_3} \end{bmatrix}.$$

Let bold numbers **1, 2, 3** correspond to the rows of [1 6 5], [6 2 4] and [5 4 3], respectively. After lengthy manipulation, one obtains

$$\delta U_1 = \int_{V_1} (\sigma_{ij}\delta\varepsilon_{ij})\,\mathrm{d}V = \sum_{m,p=0}^{\infty} [(d_{11}a_{\boldsymbol{m}} + d_{12}b_{\boldsymbol{m}} + d_{13}c_{\boldsymbol{m}})\delta a_{\boldsymbol{p}} + (d_{21}a_{\boldsymbol{m}} + d_{22}b_{\boldsymbol{m}} + d_{23}c_{\boldsymbol{m}})\delta b_{\boldsymbol{p}} + (d_{31}a_{\boldsymbol{m}} + d_{32}b_{\boldsymbol{m}} + d_{33}c_{\boldsymbol{m}})\delta c_{\boldsymbol{p}}] \tag{12}$$

where

$$d_{IJ} = g_{IJ} : \beta \tag{13}$$

$$g_{11} = \begin{pmatrix} 1 & 6 & 5 \\ 1 & 6 & 5 \end{pmatrix}_g \qquad g_{12} = \begin{pmatrix} 1 & 6 & 5 \\ 6 & 2 & 4 \end{pmatrix}_g \qquad \cdots \qquad g_{33} = \begin{pmatrix} 5 & 4 & 3 \\ 5 & 4 & 3 \end{pmatrix}_g$$

$$\beta_{ij} = \int_{V_1} X_{\boldsymbol{m}}X_{\boldsymbol{p}}\frac{m_i}{x_i}\frac{p_j}{x_j}\,\mathrm{d}V. \tag{14}$$

On the other hand, we have

$$\int_{V_3}(\sigma_{ij}-\sigma_{ij}^{\infty})\delta\varepsilon_{ij}\,\mathrm{d}V+\int_{S_r^+}\sigma_{ij}^{\infty}n_i\delta u_j\,\mathrm{d}S=\sum_{m,p=0}^{\infty}[(D_{11}A_m+D_{12}B_m+D_{13}C_m)\delta A_p+(D_{21}A_m+D_{22}B_m+D_{23}C_m)\delta B_p+(D_{31}A_m+D_{32}B_m+D_{33}C_m)\delta C_p]-\sum_{p=0}^{\infty}[\delta A_p\ \delta B_p\ \delta C_p]\sigma^{\infty}T_p \tag{15}$$

where

$$D_{IJ}=G_{IJ}:\tilde{\beta} \tag{16}$$

$$G_{11}=\begin{pmatrix}1&6&5\\1&6&5\end{pmatrix}_G\qquad G_{12}=\begin{pmatrix}1&6&5\\6&2&4\end{pmatrix}_G\qquad\cdots\qquad G_{33}=\begin{pmatrix}5&4&3\\5&4&3\end{pmatrix}_G$$

$$\tilde{\beta}_{ij}=\bar{\beta}_{ij}+\alpha_m\alpha_p\zeta_{ij}+(m_i\alpha_p\beta_{ij}^{*}+p_j\alpha_m\beta_{ji}^{*}) \tag{17}$$

$$\bar{\beta}_{ij}=\int_{V_3}\bar{X}_m\bar{X}_p\frac{m_i}{x_i}\frac{p_j}{x_j}\,\mathrm{d}V \tag{18}$$

$$\zeta_{ij}=\int_{V_3}\bar{X}_m\bar{X}_p\frac{x_ix_j}{r^4}\,\mathrm{d}V \tag{19}$$

$$\beta_{ij}^{*}=\int_{V_3}\bar{X}_m\bar{X}_p\frac{x_j}{x_i}\frac{1}{r^2}\,\mathrm{d}V \tag{20}$$

$$\bar{X}_m=(r^{m+n+k})^{-1}\sin^{m+n}\theta\cos^k\theta\sin^n\phi\cos^m\phi \tag{21}$$

$$T_p=[T_{1001}^{p}\ T_{1010}^{p}\ T_{0100}^{p}]^{\mathrm{T}} \tag{22}$$

$$T_{mnkl}^{p}=R^{2-(p+q+s)}\int_0^{2\pi}\int_0^{\pi}\sin^{m+p+q+1}\theta\cos^{n+s}\theta\sin^{k+q}\phi\cos^{l+p}\phi\,\mathrm{d}\theta\mathrm{d}\phi \tag{23}$$

$$\sigma^{\infty}=\begin{bmatrix}\sigma_{11}^{\infty}&\sigma_{12}^{\infty}&\sigma_{13}^{\infty}\\\sigma_{21}^{\infty}&\sigma_{22}^{\infty}&\sigma_{23}^{\infty}\\\sigma_{31}^{\infty}&\sigma_{32}^{\infty}&\sigma_{33}^{\infty}\end{bmatrix}$$

where θ, ϕ are the Euler angles along the longitudinal and latitudinal directions, respectively. The deformation energy of the interface layer is U_2,

$$\delta U_2=\sum_{m,p=0}^{\infty}[(\Gamma_{11}\tilde{A}_m+\Gamma_{12}\tilde{B}_m+\Gamma_{13}\tilde{C}_m+H_1)\delta\tilde{A}_p+(\Gamma_{21}\tilde{A}_m+\Gamma_{22}\tilde{B}_m+\Gamma_{23}\tilde{C}_m+H_2)\delta\tilde{B}_p+(\Gamma_{31}\tilde{A}_m+\Gamma_{32}\tilde{B}_m+\Gamma_{33}\tilde{C}_m+H_3)\delta\tilde{C}_p]R^2a^2/h \tag{24}$$

$$\Gamma_{11}=\int_0^{2\pi}\int_0^{\pi}\tilde{X}_m\tilde{X}_p(E_r\sin^2\theta+G_\theta\cos^2\theta+G_\phi\tan^2\phi)\cos^2\phi\sin\theta\,\mathrm{d}\theta\mathrm{d}\phi$$

$$\Gamma_{12}=\int_0^{2\pi}\int_0^{\pi}\tilde{X}_m\tilde{X}_p(E_r\sin^2\theta+G_\theta\cos^2\theta-G_\phi)\sin\phi\cos\phi\sin\theta\,\mathrm{d}\theta\mathrm{d}\phi$$

$$\Gamma_{13}=\int_0^{2\pi}\int_0^{\pi}\tilde{X}_m\tilde{X}_p(E_r-G_\theta)\sin^2\theta\cos\theta\cos\phi\,\mathrm{d}\theta\mathrm{d}\phi \tag{25}$$

$$\Gamma_{22} = \int_0^{2\pi}\int_0^{\pi} \tilde{X}_m\tilde{X}_p(E_r \sin^2\theta + G_\theta \cos^2\theta + G_\phi \cot^2\phi)\sin^2\phi \sin\theta \,\mathrm{d}\theta\mathrm{d}\phi$$

$$\Gamma_{23} = \int_0^{2\pi}\int_0^{\pi} \tilde{X}_m\tilde{X}_p(E_r - G_\theta)\sin^2\theta\cos\theta\sin\phi \,\mathrm{d}\theta\mathrm{d}\phi$$

$$\Gamma_{33} = \int_0^{2\pi}\int_0^{\pi} \tilde{X}_m\tilde{X}_p(E_r \cos^2\theta + G_\theta \sin^2\theta)\sin\theta \,\mathrm{d}\theta\mathrm{d}\phi.$$

Here $\Gamma_{ij} = \Gamma_{ji}$ $(i, j = 1, 2, 3)$

$$\begin{aligned} H_1 = \int_0^{2\pi}\int_0^{\pi} \{&\varepsilon_{1j}^{\infty} n_j(E_r \sin^2\theta + G_\theta \cos^2\theta + G_\phi \tan^2\phi)\cos^2\phi \\ &+ \varepsilon_{2j}^{\infty} n_j(E_r \sin^2\theta + G_\theta \cos^2\theta - G_\phi)\sin\phi\cos\phi \\ &+ \varepsilon_{3j}^{\infty} n_j(E_r - G_\theta)\sin\theta\cos\theta\cos\phi\}\tilde{X}_p \sin\theta \,\mathrm{d}\theta\mathrm{d}\phi \end{aligned} \tag{26}$$

$$\begin{aligned} H_2 = \int_0^{2\pi}\int_0^{\pi} \{&\varepsilon_{1j}^{\infty} n_j(E_r \sin^2\theta + G_\theta \cos^2\theta - G_\phi)\sin\phi\cos\phi \\ &+ \varepsilon_{2j}^{\infty} n_j(E_r \sin^2\theta + G_\theta \cos^2\theta + G_\phi \cot^2\phi)\sin^2\phi \\ &+ \varepsilon_{3j}^{\infty} n_j(E_r - G_\theta)\sin\theta\cos\theta\sin\phi\}\tilde{X}_p \sin\theta \,\mathrm{d}\theta\mathrm{d}\phi \end{aligned} \tag{27}$$

$$\begin{aligned} H_3 = \int_0^{2\pi}\int_0^{\pi} \{&\varepsilon_{1j}^{\infty} n_j(E_r - G_\theta)\sin\theta\cos\theta\cos\phi \\ &+ \varepsilon_{2j}^{\infty} n_j(E_r - G_\theta)\sin\theta\cos\theta\sin\phi \\ &+ \varepsilon_{3j}^{\infty} n_j(E_r \cos^2\theta + G_\theta \sin^2\theta)\}\tilde{X}_p \sin\theta \,\mathrm{d}\theta\mathrm{d}\phi \end{aligned} \tag{28}$$

$$\tilde{X}_m = \sin^{m+n}\theta \cos^k\theta \sin^n\phi \cos^m\phi. \tag{29}$$

$\tilde{A}_m$, $\tilde{B}_m$ and $\tilde{C}_m$ can be represented as follows:

$$\begin{aligned} \tilde{A}_m &= R^{-(m+n+k+1)}A_m - a^{m+n+k-1}a_m \\ \tilde{B}_m &= R^{-(m+n+k+1)}B_m - a^{m+n+k-1}b_m \\ \tilde{C}_m &= R^{-(m+n+k+1)}C_m - a^{m+n+k-1}c_m \end{aligned} \tag{30}$$

and n_i is the outside unit normal of the spherical surface. Using the virtual work principle, one can get a set of linear algebraic equations about the unknown coefficients a_{mnk} and A_{mnk}. Therefore the stress and strain fields of the sliding inclusion can be accurately calculated.

3. Self-consistent model for sliding polycrystals

The sliding polycrystal is considered as the aggregate of numerous randomly orientated grains with imperfect grain boundaries.

Macroscopic stress and strain rates associated with the aggregate polycrystals are denoted by $\dot{\Sigma}$ and $\dot{E}$. We have

$$\dot{\Sigma} = L\dot{E}. \tag{31}$$

For a perfect interface, the macro stress and strain rates are the volume average of the corresponding stress and strain in the single crystal constituents. For the case of an imperfect interface, there are displacement discontinuities across the grain boundary. From the average strain theorem, it follows that

$$\dot{E}_{ij} = \{\dot{\varepsilon}_{ij}\} + \dot{E}^*_{ij} \tag{32}$$

$$\dot{E}^*_{ij} = \frac{1}{2V}\int_{S_{\text{in}}} ([u_i]n_j + [u_j]n_i)\,\mathrm{d}S. \tag{33}$$

Here $\{\dot{\varepsilon}_{ij}\}$ is the volume average of the strain rate in the single-crystal constituents and $\dot{E}^*_{ij}$ is the volume average of the strain rate in the interface layers. In equation (33), the integral is taken over all interfaces.

According to the self-consistent method of Hill, the stress and strain rates in an individual grain can be calculated by replacing the grain under consideration by an equivalent spherical grain which is embedded in an infinite homogeneous matrix where instantaneous moduli are the overall moduli of the aggregate polycrystal.

As Eshelby [16] pointed out, the stress and strain rates in the equivalent spherical inclusion, $\dot{\sigma}_c$ and $\dot{\varepsilon}_c$ will be uniform if the interface is perfectly bounded,

$$\dot{\boldsymbol{\sigma}}_c = \boldsymbol{L}_c\dot{\boldsymbol{\varepsilon}}_c \tag{34}$$

$$\dot{\boldsymbol{\varepsilon}}_c = \boldsymbol{A}_c\dot{\boldsymbol{E}}. \tag{35}$$

For the imperfect grain boundary, the stress and strain in the inclusion is no longer uniform. Based on the solutions of the sliding inclusion problems, one can get the following relation:

$$\dot{\bar{\boldsymbol{\varepsilon}}}_c = \boldsymbol{A}_c\dot{\boldsymbol{E}} \tag{36}$$

$$\dot{\tilde{\boldsymbol{\varepsilon}}}_c = \tilde{\boldsymbol{A}}_c\dot{\boldsymbol{E}} \tag{37}$$

and

$$(\dot{\bar{\varepsilon}}_c)_{ij} = \frac{1}{V_\Omega}\int_\Omega \dot{\varepsilon}_{ij}\,\mathrm{d}V = \frac{1}{V_\Omega}\int_{S_i} (\dot{u}_i^- n_j + \dot{u}_j^- n_i)\,\mathrm{d}S \tag{38}$$

$$(\dot{\tilde{\varepsilon}}_c)_{ij} = \frac{1}{V_\Omega}\int_{S_i} (\dot{u}_i^+ n_j + \dot{u}_j^+ n_i)\,\mathrm{d}S \tag{39}$$

where Ω is the domain occupied by the grain, S_i is the surface of the Ω, and n_i is the unit normal of the surface S_i. It is clear that the $\dot{\bar{\varepsilon}}_c$ is the average strain of the grain, and $\dot{\tilde{\varepsilon}}_c$ is the average strain of the grain and the interface layer including the grain boundary sliding and expansion.

The average stress $\dot{\bar{\sigma}}_c$ of single-crystal constituents becomes

$$\dot{\bar{\boldsymbol{\sigma}}}_c = \boldsymbol{L}_c\dot{\bar{\boldsymbol{\varepsilon}}}_c = \boldsymbol{L}_c\boldsymbol{A}_c\dot{\boldsymbol{E}}. \tag{40}$$

The macroscopic stress rate $\dot{\boldsymbol{\Sigma}}$ is taken to be the volume average of the stress rate of the single-crystal constituents,

$$\dot{\boldsymbol{\Sigma}} = \{\boldsymbol{L}_c\boldsymbol{A}_c\}\dot{\boldsymbol{E}}. \tag{41}$$

Comparing equations (31) and (41), we obtain

$$\boldsymbol{L} = \{\boldsymbol{L}_c\boldsymbol{A}_c\}. \tag{42}$$

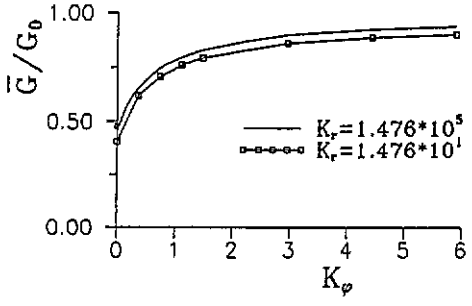

Figure 3. Relationship of overall shear modulus plotted against different boundary sliding parameters. G_0 is the overall shear modulus with non-sliding grain boundaries $K_r = E_r a/Eh$, $K_\phi = G_\phi a/Eh$.

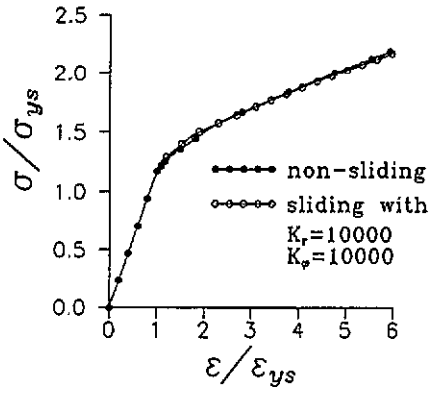

Figure 4. Tensile-stress–strain curves for sliding and non-sliding boundaries (Taylor hardening, $h_0/G = 0.1$).

4. Elastic–plastic behaviour of sliding polycrystals

Now we are ready to calculate the stress–strain relations of the sliding polycrystals based on the elastic–plastic properties of the single-crystal constituents.

A three-dimensional simulation will obviously take too much computation time. For the sake of simplification, a two-dimensional model of an aggregate polycrystal is introduced in this paper which is similar to the models proposed by Rice *et al* [17] and Mohan *et al* [18].

Each single crystal in the two-dimensional model contains three equivalent slip systems (altogether six slip systems, including reverse slip systems). Each slip system is reduced from a pair of crystallographic slip systems in an FCC crystal. If the FCC crystal has the initial yield stress τ_0 associated with each slip system, then the initial yield stresses of the equivalent slip systems in the two-dimensional model will be equal to $2\tau_0/\sqrt{3}$, $2\tau_0/\sqrt{3}$ and $\sqrt{3}\tau_0$, respectively.

Meanwhile, all single-crystal constituents have a common crystal axis [101], which is parallel to the z axis in the two-dimensional model of the aggregate polycrystal.

In order to prove the validity of the two-dimensional model, tension stress–strain relations for the FCC polycrystal are first calculated under the classical situation of perfect interface bonding.

Figure 2 shows the results of the calculation for the FCC polycrystal with randomly orientated, non-hardening single crystals. The curve marked with full circles indicates the calculated results of Hill's model for the three-dimension simulation given by Hutchinson [3]. The curve marked with open circles represents the present results of the two-dimensional model. In the early stages of deformation, the predictions of the two-dimensional model are slightly higher than that of the three-dimensional simulation, due to the constraint of the plane-strain condition. As the plastic deformation increases, the predictions of two models are essentially identical.

4.1. Elastic constants of FCC polycrystals with imperfect grain boundaries

We now calculate the elastic constants of the FCC sliding polycrystal made of cylindrical grains. For a FCC single crystal, the elastic modulus tensor in the crystal axes can be specified

by three parameters η_1, η_2 and η_3 due to the cubic symmetry. The instantaneous overall moduli of the FCC polycrystal in the two-dimensional model display transverse isotropy with respect to the z axis so that the non-zero independent moduli are

$$L = \begin{bmatrix} L_{11} & L_{12} & L_{13} & 0 & 0 & 0 \\ L_{12} & L_{11} & L_{13} & 0 & 0 & 0 \\ L_{13} & L_{13} & L_{33} & 0 & 0 & 0 \\ 0 & 0 & 0 & L_{44} & 0 & 0 \\ 0 & 0 & 0 & 0 & L_{44} & 0 \\ 0 & 0 & 0 & 0 & 0 & L_{66} \end{bmatrix} \tag{43}$$

where $L_{66} = \frac{1}{2}(L_{11} - L_{12})$.

In the case of plane strain, we have

$$\gamma_{zx} = \gamma_{yz} = 0 \qquad \varepsilon_z = 0. \tag{44}$$

In the two-dimensional model, all slip systems are in plane systems, so that

$$\gamma^{\mathrm{p}}_{zx} = \gamma^{\mathrm{p}}_{yz} = 0 \qquad \varepsilon^{\mathrm{p}}_z = 0. \tag{45}$$

From equations (44) and (45), one arrives at

$$\varepsilon^{\mathrm{e}}_z = (1/E_3)[\sigma_z - \nu_3(\sigma_x + \sigma_y)] = 0 \qquad \sigma_z = \nu_3(\sigma_x + \sigma_y)$$

where E_3 and ν_3 are the elastic modulus and Poisson's ratio of the polycrystal in the z axis direction, respectively. Obviously the out-plane overall elastic modulus and Poisson's ratio in the two-dimensional model are equal to the out-plane elastic modulus and Poisson's ratio of the single-crystal constituents.

We introduce the two-dimensional stress vector $\sigma = [\sigma_{11}\ \sigma_{22}\ \tau_{12}]^{\mathrm{T}}$ and strain vector $\varepsilon = [\varepsilon_{11}\ \varepsilon_{22}\ \gamma_{12}]^{\mathrm{T}}$ for the two-dimensional model. The non-zero instantaneous elastic moduli are

$$L = \begin{bmatrix} L_{11} & L_{12} & 0 \\ L_{21} & L_{22} & 0 \\ 0 & 0 & L_{66} \end{bmatrix}. \tag{46}$$

The in-plane overall shear modulus $\bar{G}$ and Poisson's ratio $\bar{\nu}$ can be evaluated as follows:

$$\bar{G} = \tfrac{1}{2}(L_{11} - L_{12}) \qquad \bar{\nu} = L_{12}/(L_{11} + L_{12}). \tag{47}$$

The calculation has been carried out for a sliding polycrystal made of Al-single-crystal constituents with parameters $\eta_1 = 76.9$ GPa, $\eta_2 = 23.5$ GPa, $\eta_3 = 28.5$ GPa. The calculated results of overall shear modulus are shown in figure 3. The full curve indicates the results for very stiff normal interface modulus, while the small squares represent the results for moderate stiff interface normal elastic modulus. It is clear that when the interface tangential shear modulus G_ϕ tends to zero, the relative overall shear modulus $\bar{G}/G_0$ will approach 0.46 for $K_r = 1.476 \times 10^5$. This value is slightly lower than the value 0.54 given by Yang *et al* [15] for free sliding aggregate polycrystals made of cubic grains. Cubic grains possess edges and corners, while cylindrical grains have smooth boundaries. Obviously the present aggregate polycrystal made of cylindrical grains slides more easily along grain boundaries. This results in the reduction of overall shear modulus $\bar{G}$. Here G_0 represents the overall shear modulus of the polycrystal with perfect grain boundaries.

4.2. The concentration factor tensor

We now introduce two non-dimensional parameters: $K_r = E_r a/Eh$, $K_\phi = G_\phi a/Eh$ where a is the radius of a cylindrical grain, and h is the thickness of the interface layer. E_r and G_ϕ are the normal elastic modulus and the tangential shear modulus of interface layers, respectively.

Using the present method, one can easily calculate the strain (or stress) concentration factor tensor A_c of the inclusion problem when both the matrix and the inclusion are isotropic or anisotropic materials. For comparison with Eshelby's solution, we choose an isotropic matrix with elastic modulus $E = 1000$ GPa and Poisson's ratio $\nu = \frac{1}{3}$. In order to simulate the perfect bonding condition, the interface layer is assumed to be extremely stiff with $K_r = 10^6$, $K_\phi = 10^6$. The calculation was carried out for the two-dimensional model.

Two types of inclusions are discussed. First, the inclusion is isotropic with $E_{in} = 900$ GPa, Poisson's ratio $\nu_{in} = \frac{1}{3}$. Using the present method and Eshelby's solution, we can get the concentration factor tensor $(A_c)_{present}$ and $(A_c)_{Eshelby}$ (see table 1).

Table 1. Concentration factor tensor.

	A_{11}	A_{22}	A_{33}
$(A_c)_{present}$	1.072	1.071	1.062
$(A_c)_{Eshelby}$	1.074	1.074	1.067

Comparing diagonal terms of $(A_c)_{present}$ with $(A_c)_{Eshelby}$, we can see that the maximum relative error is less than 0.5%. By the way, the off-diagonal terms of the concentration factor are very small compared with the diagonal terms in the above example. We can conclude that the present result for the concentration factor is essentially identical with Eshelby's accurate solution.

Second, the inclusion is anisotropic with elastic moduli $g^*_{ij} = g_{ij} + \Delta g$, where g_{ij} are isotropic elastic modulus tensor components for the Yang's modulus $E_{in} = 900$ GPa, Poisson's ratio $\nu_{in} = \frac{1}{3}$ and $\Delta g = 50$ GPa. The diagonal terms of the concentration factor tensors $(A_c)_{present}$ and $(A_c)_{Eshelby}$ are given in table 2.

Table 2. Concentration factor tensor.

	A_{11}	A_{22}	A_{33}
$(A_c)_{present}$	1.054	1.055	0.984
$(A_c)_{Eshelby}$	1.057	1.057	0.982

Here Eshelby's solution for the concentration factor was obtained using the elastic potential and the Green's function. The present calculated result for the concentration factor is in good agreement with Eshelby's solution.

When the matrix is isotropic and the inclusion is spheroidal or cylindrical, Eshelby's solutions for the concentration factor provide very simple analytical formulae. When the matrix is a general anisotropic medium, the calculation of the concentration factor of Eshelby's solution is very complicated.

The present method can easily deal with the inclusion problems with anisotropic matrix.

4.3. Elastic–plastic behaviour for sliding FCC polycrystals

In this section, two kinds of single-crystal hardening law are chosen for calculation, (1) Taylor's isotropic hardening law with $h_{\alpha\beta} = h$; (2) Asaro's hardening law with $h_{\alpha\beta} = h_0[q + (1-q)\delta_{\alpha\beta}]$,

$$h = h_0 \sec^2\left(\frac{h_0\gamma}{\tau_s - \tau_0}\right) \qquad \gamma = \sum_{\alpha=1}^{N} \gamma^{(\alpha)}.$$

We assume that all single crystals are elastic isotropic with Yang's modulus $E = 1000\tau_0$, Poisson's ratio $\nu = \frac{1}{3}$.

First we calculate the macro stress–strain curves of an aggregate polycrystal under tensile or shear loading for the classical situation of perfect bonding conditions. The calculation was carried out using the self-consistent method proposed in section 3.

In figures 4 and 5, the curves with open circles represent the present results for very stiff grain boundaries with ($K_r = 1.0 \times 10^4$, $K_\phi = 1.0 \times 10^4$), while the curves with full circles or small squares represent the results of perfect grain boundaries based on Eshelby's solution. The single crystal is assumed to obey Taylor's hardening law with $h_0 = 0.1G$. These figures clearly show that the present results are essentially identical to that of perfect grain boundaries.

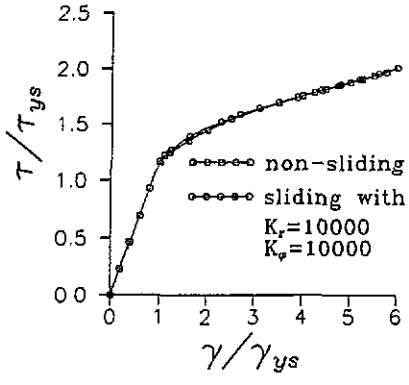

Figure 5. Shear-stress–shear-strain curves for sliding and non-sliding boundaries (Taylor hardening, $h_0/G = 0.1$).

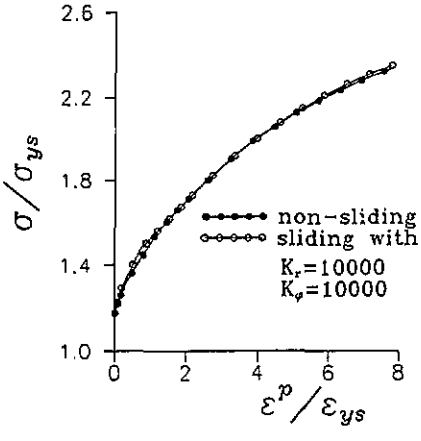

Figure 6. Tensile-stress–plastic-strain curves for sliding and non-sliding boundaries (Asaro hardening, $h_0/G = 0.1$, $q = 1.2$, $\tau_s/\tau_0 = 1.8$).

In figure 6, the open and full circles have the same meaning as above, but all single crystals obey Asaro's hardening law with $h_0 = 0.1G$, $q = 1.2$, $\tau_s/\tau_0 = 1.8$. The two curves are very close to each other.

Figure 7 contains plots of the macro responses under shear loading. The two curves are very close in the range of $0 \leqslant \gamma/\gamma_0 \leqslant 5.0$ but, as the shear loading increases further, the difference between these two curves also increases. This is due to the effect of grain boundary sliding. It means that, in order to simulate perfect bonding conditions, we need to use larger K_r and K_ϕ.

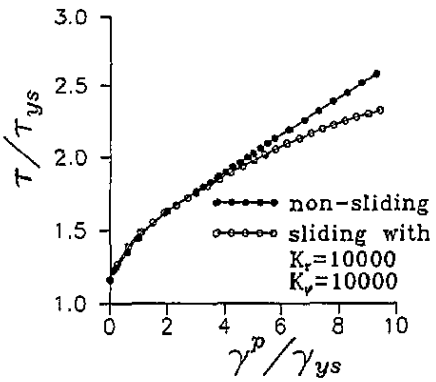

Figure 7. Shear-stress–plastic-shear-strain curves for sliding and non-sliding boundaries (Asaro hardening, $h_0/G = 0.1$, $q = 1.2$, $\tau_s/\tau_0 = 1.8$).

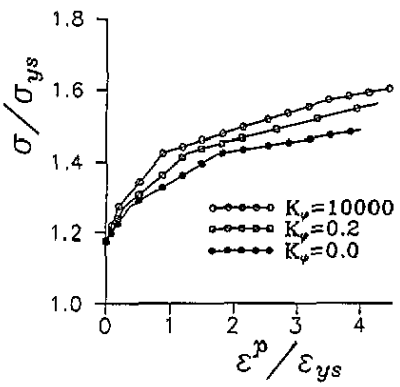

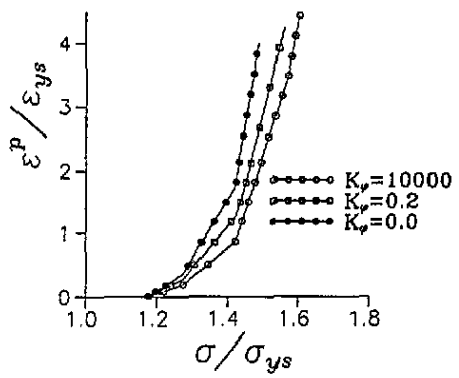

Figure 8. Tensile-stress–plastic-strain curves for different boundary sliding resistances (K_τ = 10000, Taylor hardening, $h_0/G = 0.02$).

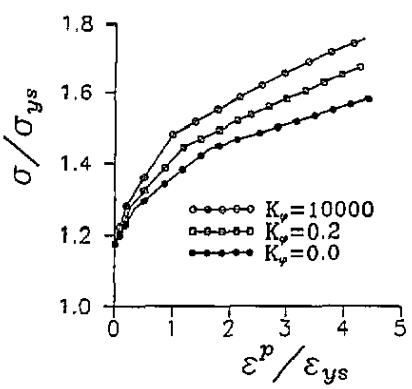

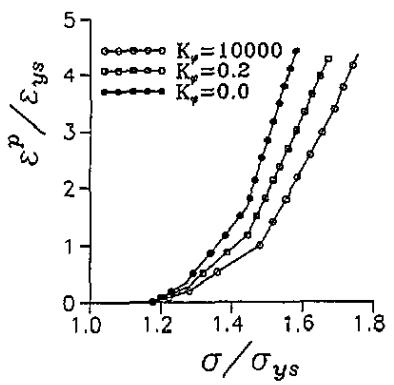

Figure 9. Tensile-stress–plastic-strain curves for different boundary sliding resistances (K_τ = 10000, Taylor hardening, $h_0/G = 0.04$).

Now we consider sliding polycrystals. Three types of grain boundaries with very stiff, moderate stiff and soft tangential shear moduli were used for calculations, while the normal

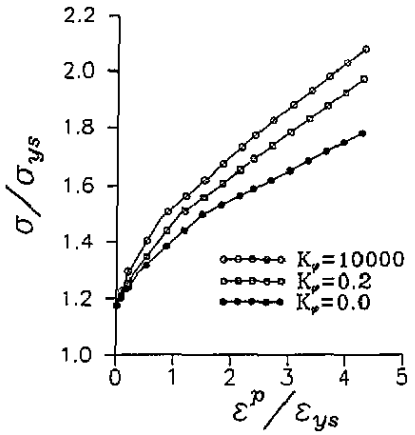

Figure 10. Tensile-stress–plastic-strain curves for different boundary sliding resistances ($K_r = 10000$, Taylor hardening, $h_0/G = 0.1$).

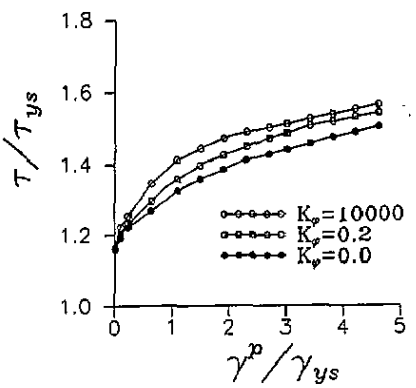

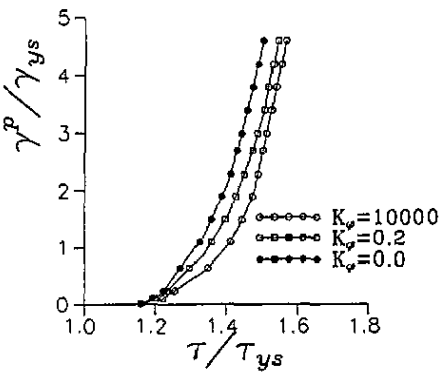

Figure 11. Shear-stress–plastic-shear-strain curves for different boundary sliding resistances ($K_r = 10000$, Taylor hardening, $h_0/G = 0.02$).

interface modulus parameter $K_r = 1.0 \times 10^4$.

The overall stress–plastic-strain curves of the aggregate polycrystal are presented in figures 8–10 for the case where all single crystals obey Taylor's isotropic hardening law with hardening parameters $h_0/G = 0.02$, 0.04, 0.1, respectively. In these figures, the open circles, squares and full circles represent the results for $K_\phi = 10^4$, 0.2 and 0.0, respectively. These three figures clearly show that the smaller the interface tangential shear modulus, the softer is the aggregate polycrystal.

Figures 11–13 indicate the plots of macro shear stress against plastic shear strain of the aggregate polycrystal subject to shear loading for the case where all single-crystal constituents also obey Taylor's isotropic hardening law with hardening parameters $h_0/G = 0.02$, 0.04, 0.1, respectively. From these figures, the same conclusions can be reached.

Figures 14 and 15 show macro stress–strain curves of the aggregate polycrystal under tension and shear loading, but the single-crystal constituents have Asaro's hardening properties with parameters $h_0 = 0.1G$, $q = 1.2$ and $\tau_s/\tau_0 = 1.8$. A similar tendency is clearly shown in these figures.

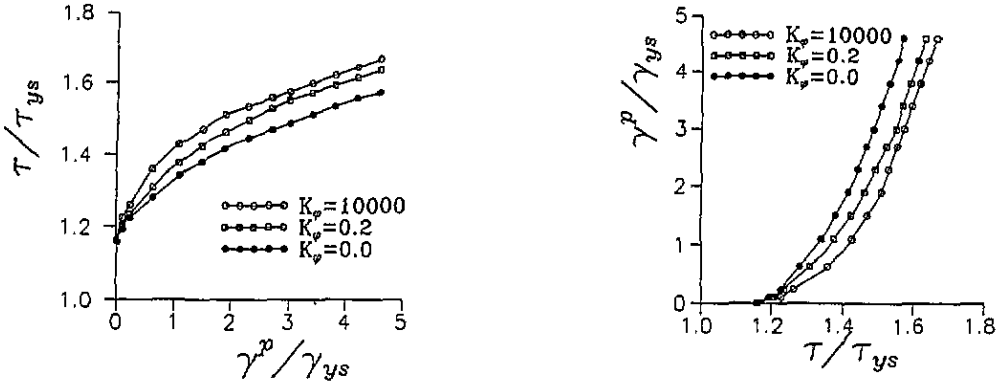

Figure 12. Shear-stress–plastic-shear-strain curves for different boundary sliding resistances ($K_r = 10000$, Taylor hardening, $h_0/G = 0.04$).

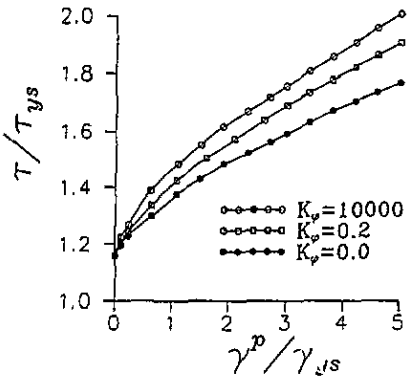

Figure 13. Shear-stress–plastic-shear-strain curves for different boundary sliding resistances ($K_r = 10000$, Taylor hardening, $h_0/G = 0.1$).

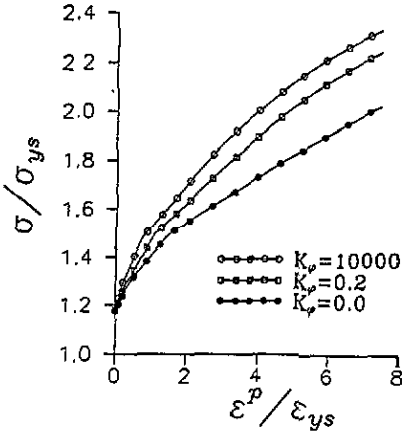

Figure 14. Tensile-stress–plastic-strain curves for different boundary sliding resistances ($K_r = 10000$, Asaro hardening, $h_0/G = 0.1$, $\tau_s/\tau_0 = 1.8$, $q = 1.2$).

General speaking, the stresses in the interface layers will increase as the tension or shear loading increases, while the stiffness of the interface layers will decrease. This means that the stiffness of the interface layers depends on deformation history. In order to simulate this mechanism, the shear-stress–shear-strain relationship of the interface layers takes the form

$$\begin{cases} \tau/\tau^0 = \gamma/\gamma^0 & \gamma \leqslant \gamma^0 \\ \tau/\tau^0 = (\gamma/\gamma^0)^n & \gamma > \gamma^0 \end{cases} \tag{48}$$

Using rate formation, we have

$$\begin{cases} \dot{\tau} = G_\phi^0 \dot{\gamma} & \gamma \leqslant \gamma^0 \\ \dot{\tau} = n(\gamma/\gamma^0)^{n-1} G_\phi^0 \dot{\gamma} & \gamma > \gamma^0. \end{cases} \tag{49}$$

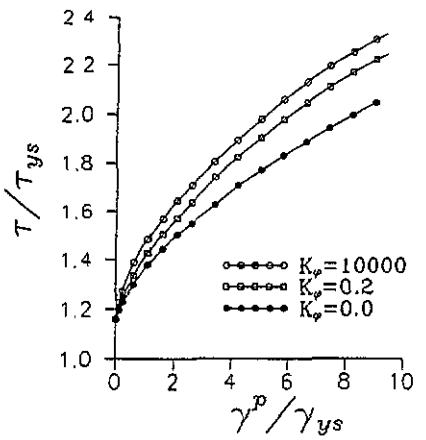

Figure 15. Shear-stress–plastic-shear-strain curves for different boundary sliding resistances ($K_r = 10000$, Asaro hardening, $h_0/G = 0.1$, $\tau_s/\tau_0 = 1.8$, $q = 1.2$).

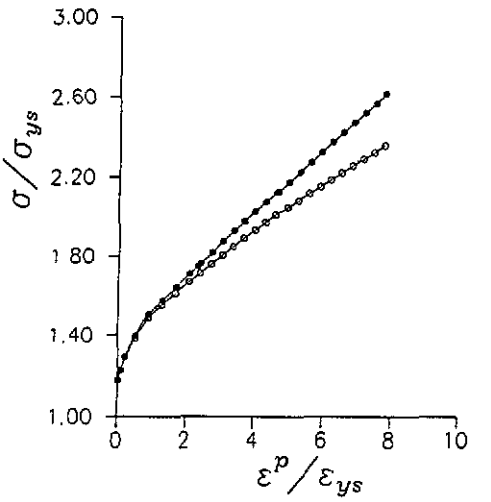

Figure 16. Tensile-stress–plastic-strain curves for different boundary sliding resistances ($K_r = 10000$, Taylor hardening, $h_0/G = 0.1$, $\tau^0/\tau_0 = 1.05$, $n = 0.1$). Open circles, K_ϕ varying as equation (49); full circles, $K_\phi = K_\phi^0 = 10$, $K_\phi^0 = G_\phi^0 a/Eh$.

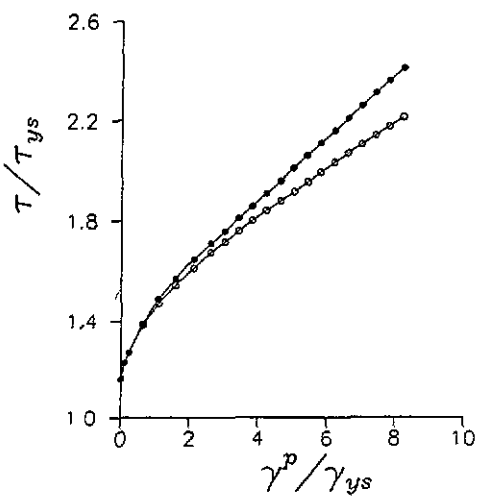

Figure 17. Shear-stress–plastic-shear-strain curves for different boundary sliding resistances ($K_r = 10000$, Taylor hardening, $h_0/G = 0.1$, $\tau^0/\tau_0 = 1.05$, $n = 0.1$). Open circles, K_ϕ varying as equation (49); full circles, $K_\phi = K_\phi^0 = 10$, $K_\phi^0 = G_\phi^0 a/Eh$.

Here, τ^0 and γ^0 are the yield shear stress and yield shear strain of the interface layers respectively, and G_ϕ^0 is the elastic tangential shear modulus of the interface layers. Figures 16 and 17 compare the results of constant interface modulus with those of an interface tangential shear modulus that varies according to equations (48) and (49). From these two figures we can see how the interface properties influence the macro behaviour of the aggregate polycrystal.

5. Conclusions

From this study one can draw the following conclusions.

1. A general analytical solution of the sliding spherical inclusion which is embedded in an infinite general anisotropic matrix is presented in this paper. The interface sliding and expansion can be easily simulated using this solution.

2. The variational method is a powerful tool for dealing with spherical inclusion problems with a general anisotropic matrix. In particular, for an imperfect interface, the variational method shows great benefits compared with the elastic potential method and the Green's function method.

3. Incorporating the above solution into the self-consistent method, a generalized self-consistent method is proposed for predicting the overall mechanical behaviour of aggregate sliding polycrystals.

4. Using the two-dimensional model of an aggregate polycrystal, the numerical calculations for the sliding polycrystals have been carried out. The numerical calculations include the elastic properties of the polycrystals, the concentration factor tensors of inclusion problems with imperfect interfaces, and the elastic–plastic behaviour of sliding polycrystals.

5. The numerical results clearly show that the sliding and expansion of the grain boundaries have significant effects on the mechanical behaviour of aggregate polycrystals.

Acknowledgment

This research was supported by The National Natural Science Foundation of China.

References

[1] Hill R 1965 *J. Mech. Phys. Solids* **13** 89
[2] Asaro R J 1983 *Adv. Appl. Mech.* **23** 1
[3] Hutchinson J W 1972 *Proc. R. Soc.* A **319** 247
[4] Hutchinson J W 1964 *J. Mech. Phys. Solids* **12** 11
[5] Nemat-Nassser S 1986 *Proc. R. Soc.* A **407** 343
[6] Krŏner E 1958 *Z. Phys.* **151** 504
[7] Budiansky B and Wu T T 1962 *Proc. 4th Congr. Appl. Mech.* p 1175
[8] Walpole L J 1978 *Math. Proc. Cambridge Phil. Soc.* **83** *495*
[9] Mura T, Jasiuk I and Tsuchida B 1985 *Int. J. Solids Struct.* **21** 1165
[10] Ghahremani F 1980 *Int. J. Solids Struct.* **16** 825
[11] Benvenise Y 1985 *Mech. Mater.* **4** 197
[12] Hashin Z 1990 *Mech. Mater.* **8** 333
[13] Luo H A and Weng G J 1990 *Mech. Mater.* **8** 77
[14] Luo H A and Chen Y 1991 *J. Appl. Mech.* **58** 428
[15] Yang W, Zhong Z and Hang K C 1991 *Proc. IUTAM Symp. on Constitutive Relations for Finite Deformation of Polycrystalline Metals, Beijing* (Berlin: Springer; Peking: Peking University Press) p 136
[16] Eshelby J D 1957 *Proc. R. Soc.* A **241** 376
[17] Rice J R, Hawk D E and Asaro R J 1990 *Int. J. Fracture* **42** 301
[18] Mohan R, Ortiz M and Shih C F 1992 *J. Mech. Phys. Solids* **40** 315